DETERMINATION OF DIAPHRAGM OPENING-TIMES AND USE OF DIAPHRAGM PARTICLE TRAPS IN A HYPERSONIC SHOCK TUBE

by

J. E. Drewry and Z. A. Walenta

JUNE 1965

UTIAS TECHNICAL NOTE NO. 90

ACKNOWLEDGEMENTS

We would like to thank Dr. G. N. Patterson for providing us with the opportunity to carry out this research at UTIAS.

The supervision and encouragement rendered to us by Dr. I. I. Glass throughout this work is very much appreciated.

The financial support received under NASA Grant NsG-633 and from the Canadian National Research Council and the Defence Research Board is gratefully acknowledged.

SUMMARY

Experimental investigations have been carried out in the UTIAS 4 in. x 7 in. hypersonic shock tube to measure diaphragm opening-times and to evaluate shock tube performance with particle traps located near the diaphragm station. Calculations, based on simple theoretical models, have been made in order to obtain approximate comparisons with the experimental results.

TABLE OF CONTENTS

NOTATION

a	sound speed (ft./sec.)
A	cross-section area (in.^{2})
b	base width of diaphragm petal (in.)
c_D	drag coefficient
d_s	diaphragm scribe depth (in.)
F	force acting on diaphragm petal (lbs.)
G	factor defined by Eq. (C.8)
I	moment of inertia of diaphragm petal
L	nondimensionalizing factor given in Eq. (B.2)
m	particle mass (slugs)
M	flow Mach number
M_s	shock Mach number
M_σ	bending moment acting on diaphragm petal
p	pressure (lb./in.^{2})
S	particle reference area (in.^{2})
T	nondimensionalizing factor given in Eq. (B.2)
u, U	flow velocity (ft./sec.)
V	particle velocity (ft./sec.)
α	flow deflection angle (Fig. B.1)
β	factor defined by Eq. (C.2)
γ	isentropic index
θ	deflection angle of diaphragm petal (Fig. A.1)
ρ	flow density (slugs/in.^{3})

ρ_d	density of diaphragm material (slugs/in.^{3})
σ	bending stress in diaphragm petal (lbs./in.^{2})
ζ_d	basic (unscribed) diaphragm thickness (in.)
ζ_s	diaphragm thickness along scribe (in.)

Subscripts

o	initial conditions
1, 2, 3, 3', 4, 4'	refer to flow regions shown in Fig. C. 1

Superscripts

'	nondimensional quantities

15772

1. INTRODUCTION

As a result of particle impact and erosion which were encountered during the initial calibration tests of the 4 in. x 7 in. combustion-driven shock tube (Refs. 1 and 2) a limited experimental program has been carried out in order to obtain information that would prove useful in overcoming this problem. The investigation consisted of (1) measurements of the time required for shock tube diaphragms to rupture and (2) an evaluation of shock tube performance when a system of diaphragm particle traps were located just downstream of the diaphragm station.

Two simultaneous and independent measurements of diaphragm opening-times were made in order to try to establish a reasonable working value which may be used in some future design of a quick-opening, shock-generating valve to replace shock tube diaphragms. Such a device would greatly enhance shock tube operation.

The use of an optically-tight system of traps provide a possible means for removing diaphragm particles from shock tube flows. Such a trap system was designed and tested in the present work, with particular emphasis given to the determination of its effect on the overall performance of the shock tube.

Author

2. MEASUREMENT OF DIAPHRAGM OPENING-TIMES

The general experimental set-up which was used is shown schematically in Fig. 1.

The diaphragms used in these tests were cut from stainless steel sheet (type 302) and were scribed in the manner shown in Fig. 2a. A typical ruptured diaphragm is shown in Fig. 2b.

Measurements of diaphragm opening-times were made by two different methods. One measurement was taken by using a Philips OAP-12 photodiode to observe an increase in light emission from the driver section as the diaphragm ruptured. The hot combustion-driver gas served as the source of light emission. The photodiode probe which was used is shown in Fig. 3.

A second measurement of diaphragm.opening-time was taken by means of a Shure Model MC11-J microphone attached to the outer wall of the shock tube at the diaphragm station as shown in Fig. 1.

Signals from the two sensing devices were fed into a dual beam oscilloscope and recorded simultaneously. The results from two tests are shown in Fig. 4. In Fig. 4a the photodiode probe was facing up-

stream along the centerline of the shock tube (i.e., looking directly at the diaphragm). In Fig. 4b the probe was rotated 90° from the above position and thus was sensing side wall reflection only. The passage of the shock wave is clearly indicated when the probe is in this position. The lower trace in each figure is the signal received from the microphone. The period of "diaphragm noise" is seen to be in good agreement with the time required to reach peak light intensity in the photodiode traces.

Further experimental results are shown in Fig. 5. In Fig. 5a the photodiode response corresponds to the same mode of operation used to obtain the results of Fig. 4a. In Fig. 5b the viewing field of the photodiode was collimated by placing Trap A (see Fig. 7) just downstream of the diaphragm station. When the diaphragm opening-area passes beyond this viewing area, the photodiode output ceases to increase and remains quite constant up to the time of shock wave arrival at the probe. Thus it was concluded that changes in light intensity corresponded to the opening of the diaphragm only and not to deviations in background illumination. The measured risetime in Fig. 5a was 845 μsec. as compared to 710 μsec. for Fig. 5b.

The microphone signal in Fig. 5a was very noisy as a result of insecure mounting. An improved method of mounting resulted in the response shown in Fig. 5b as well as that shown in Fig. 4.

The photodiode response may also be correlated with the pressure-time history for the combustion-driver gas as seen in Fig. 6. The oscilloscope triggering signal for the photodiode was delayed for 14 msec. after the triggering signal for the pressure transducer (Kistler Model 605) used to measure combustion-driver pressure. The photodiode response is seen to begin just prior to the time of peak combustion pressure. This is to be expected in the present system since the pressure transducer is located in the end of the driver section at a distance of 7.75 feet away from the diaphragm station.

The experimental values for diaphragm opening-times which were measured in this work are given in Table I. Most of the results obtained are for diaphragms having a basic thickness, τ_d, of .108" and a scribe depth, d_s, of .048". The combustion-driver pressure necessary to rupture these diaphragms was approximately 2000 psi. The average values obtained for the opening-time of these diaphragms were:

Photodiode - 800 $\pm$ 45 μsec.

Microphone - 850 $\pm$ 25 μsec.

A simple model for diaphragm rupture was assumed for the purpose of calculating approximate theoretical values with which to compare

the results given in Table I. A detailed discussion of this analysis is given in Appendix A. The following simple relation was obtained for total diaphragm opening-time

$$t = 4.73 \left[\frac{\rho_d b \tau}{p_4}\right]^{\frac{1}{2}} \times 10^4 \quad (\mu\text{sec.}) \qquad (2.1)$$

where

ρ_d = density of diaphragm material (lb./in.^{3})

b = base width of diaphragm petal (in.)

τ = diaphragm thickness (in.)

p_4 = combustion-driver pressure (lb./in.^{2})

Results of a diaphragm opening analysis made at NASA Ames Research Center (Ref. 3) were received just after the present theoretical study was completed. In the Ames analysis it was assumed (as in the present work) that each diaphragm petal of a four-lobe opening acted as a freely-hinged leaf exposed to a constant pressure. Their final expression (using the present notation) for diaphragm opening-time was

$$t = 1.085 \left[\frac{\rho_d b \tau}{p_4}\right]^{\frac{1}{2}} \times 10^3 \quad (\mu\text{sec.}) \qquad (2.2)$$

where ρ_d was taken in units of lb./ft.^{3} instead of lb./in.^{3} as in Eq.(2.1). Making the appropriate conversion of units in Eq. (2.2) gives the following result

$$t = 4.51 \left[\frac{\rho_d b \tau}{p_4}\right]^{\frac{1}{2}} \times 10^4 \quad (\mu\text{sec.}) \qquad (2.3)$$

which is in good agreement with Eq. (2.1).

3. SHOCK TUBE PERFORMANCE WITH DIAPHRAGM PARTICLE TRAPS

The set of particle traps which was used in this work is shown in Fig. 7. A discussion of design features and considerations for these traps is given in Appendix B.

The overall evaluation of shock tube performance is based mainly on measurements of shock Mach number in the test section as a function of initial conditions. Stagnation-point heat transfer rate measurements (Ref. 4) were also made in order to determine test flow duration and uniformity.

Results of the shock speed measurements are given in Fig. 8, where the variation in shock Mach number over a range of diaphragm pressure ratios is plotted for different particle trap arrangements. A decrease in shock Mach number for a given value of p_4/p_1 is evident when more than one of the traps are present in the tube. It should be noted that no correction has been made for overall shock wave attenuation in the driven section. Such a correction would, of course, provide better agreement between the experimental results and theoretical predictions.

The measurements corresponding to operation with only the first-stage trap (Trap A) in position appear to fall within the scatter of the results obtained during normal operation (i.e., without particle traps). However, as mentioned above, when additional traps are placed in the tube there is a noticeable decrease in shock tube performance.

As in the case of diaphragm opening-time considerations, a simple theoretical model was used as a means of making an approximate determination of shock tube performance when flow obstacles were located near the diaphragm (Ref. 5). A detailed discussion of this simplified analysis is given in Appendix C.

The calculated performance curves are shown in Fig. 9. All of the experimental results given in Fig. 8 have been arbitrarily corrected in Fig. 9 by an amount equal to an average shock Mach number attenuation ($\overline{\Delta M}_s = 1.24$) for operation without traps which is based on the average deviation between the experimental data and ideal theory, (see Eq. C.12). In other words, the results of Fig. 8 have been shifted to the right in Fig. 9 to provide agreement between theory and experiment for operation without traps. This adjustment then makes it possible to have a more direct comparison of theory and experiment for operation with traps.

The experimental results, as shown in Fig. 9, indicate that the effect of a single flow obstacle (viz., Trap A) is not as severe as predicted by the simple theory. The results corresponding to operation with two or three particle traps are in somewhat better agreement with theoretical predictions.

Some typical thin-film surface temperature and heat transfer rate measurements (Ref. 4), which were taken at the stagnation line of a right circular cylinder (0.5" dia.), are shown in Fig. 10. These results were obtained using initial pressures, p_1, of 20 mm Hg in the first two cases and 40 mm Hg in the latter case with combustion-driver pressures of approximately 2000 psi in all three cases.

Figure 10a shows the results obtained during conventional operation without particle traps. The results given in Fig. 10b were taken during operation with the complete set of particle traps located in the shock

tube as shown in Fig. 7. Figure 10c gives the results obtained while operating with three traps as above but at a lower value of diaphragm pressure ratio and hence a lower value of shock Mach number.

As may be seen from the results of Fig. 10 there is very little apparent change in the flow uniformity from Fig. 10a to Fig. 10b. There is a slight increase in test flow duration which may be attributed to the decrease in shock Mach number. However, in Fig. 10c noticeable evidence of flow nonuniformity appears after approximately 150 microseconds of test flow. This flow disturbance appears to be in the form of a weak shock or compression wave which has been caused by the traps and swept downstream ahead of the contact region. The data given in Fig. 9 also indicates an increase in the attenuating effect of the traps on the flow when the initial pressure is increased from 20 to 40 mm Hg for the case of three particle traps.

It would have been helpful to have carried out schlieren or interferometric studies of the flow field in the test section in order to better evaluate the overall effect of the particle traps on shock tube performance. However, due to time limitations this was not possible.

As for the particle problem itself, the primary source of particles which were causing the damage reported in Ref. 1 was found to be from secondary cellophane diaphragms being used to provide buffered (argon) operation of the shock tube. Particles resulting from the primary diaphragm do exist, but in much smaller size and quantity than thought when this work was initiated. Evidence of the cumulative damage caused by these particles during some 25 or 30 runs without particle traps is seen on the surface of the photodiode probe in Fig. 3. However, this is not considered to be a real problem provided the tube is cleaned by shock waves produced by low pressure cold runs to remove any debris existing after a hot run. The latter operation has proved effective and can be recommended.

There was some indication that the particle trap system did result in some decrease of primary diaphragm particles. However, it is felt that, since the damage in tests without traps was quite low and somewhat sporadic, any evaluation of the overall effectiveness of the particle traps in terms of diaphragm particle removal is not justified on the basis of the limited number of tests carried out in the present work.

4. CONCLUDING REMARKS

Experimental measurements have been carried out in a hypersonic shock tube to determine diaphragm opening-times. Measurements have also been made for the purpose of evaluating shock tube

performance when diaphragm particle traps were located near the diaphragm station. Simple theoretical models were used as a means of obtaining approximate comparisons with the experimental results.

Diaphragm opening-times of the order of 800 microseconds were measured for diaphragms having basic thicknesses ranging from .062" to .176". Approximate theoretical calculations gave values of the order of 400 microseconds. It is felt that this considerable disagreement is, to a large extent, due to the use of an over-simplified theoretical model for diaphragm rupture.

The experimental results which were obtained during the evaluation of shock tube performance with a system of particle traps located just downstream of the diaphragm indicated a noticeable decrease in overall performance. The attenuating effect of the traps became stronger with increasing channel pressure p_1 for a fixed driver pressure p_4 during operation with the complete set of traps. Some evidence of flow nonuniformity was also observed at the highest value (40 mm Hg) of p_1.

REFERENCES

1. Boyer, A.G. Drewry, J.E. — 4" x 7" Hypersonic Shock Tube Calibration and Performance, UTIAS Annual Progress Report, 1963, Section C-4.

2. Boyer, A.G. — Design, Instrumentation and Performance of the UTIAS 4-in. x 7-in. Hypersonic Shock Tube, May 1965, UTIAS Report No. 99.

3. ---------- — Private Communication from Hypersonic Shock Tunnel Group at NASA, Ames.

4. Walenta, Z.A. — Analogue Networks for High Heat Transfer Rate Measurements, UTIAS Technical Note No. 84, November 1964.

5. Russell, D.A. — A Study of Area Change Near the Diaphragm of a Shock Tube, GALCIT Hypersonic Research Project, Memorandum No. 57, July 1960.

6. Nagamatsu, H.T. — Shock Tube Technology and Design, General Electric Research Laboratory, Report No. 58-RL-2107, November 1958.

7. Resler, E.L. Lin, Shao-Chi Kantrowitz, A. — The Production of High Temperature Gases in Shock Tubes, Journal of Applied Physics, Vol. 23, No. 12, December 1952.

8. Schultz, D.L. — A Note on the Use of Steady Expansions in Shock Tubes and Shock Tunnels, A.R.C. 22, 511-Hyp. 155, January 1961.

9. Friend, W.H. — The Interaction of a Plane Shock Wave with an Inclined Perforated Plate, UTIAS Technical No. 25, October 1958.

10. Glass, I.I. Hall, J.G. — Handbook of Supersonic Aerodynamics, Section 18, Shock Tubes, NAVORD Report 1488 (Vol. 26), December 1959.

11. Schlichting, H. — Boundary Layer Theory, Pergamon Press, 1955.

TABLE I

RESULTS OF DIAPHRAGM OPENING-TIME MEASUREMENTS

Basic Diaphragm Thickness, τ_d (in)	Thickness Along Scribe, τ_s [a] (in)	Combustion-Driver Pressure, p_4 (psi)	Photodiode Result, t_p (μsec)	Microphone Result, t_m (μsec)	Theoretical Value [b]	
					Based on τ_d (μsec)	Based on τ_s (μsec)
.176	.122	3690	704	x	400	333
.176	.122	3830	x	660	393	327
.108	.060	2140	820	x	411	306
.108	.060	2140	770	x	411	306
.108	.060	1915	845	845	435	324
.108	.060	1865	800	852	440	328
.108	.060	1875	x	875	439	327
.108	.060	1955	760	846	430	320
.108	.060	1860	x	833	441	329
.062	.036	930	792	797	473	360

a) $\tau_s = \tau_d - d_s$

b) Diaphragm parameters: $\rho_d = .282\ \mathrm{lb/in^3}$; $b = 5.3$ in.

x - experimental result not obtained

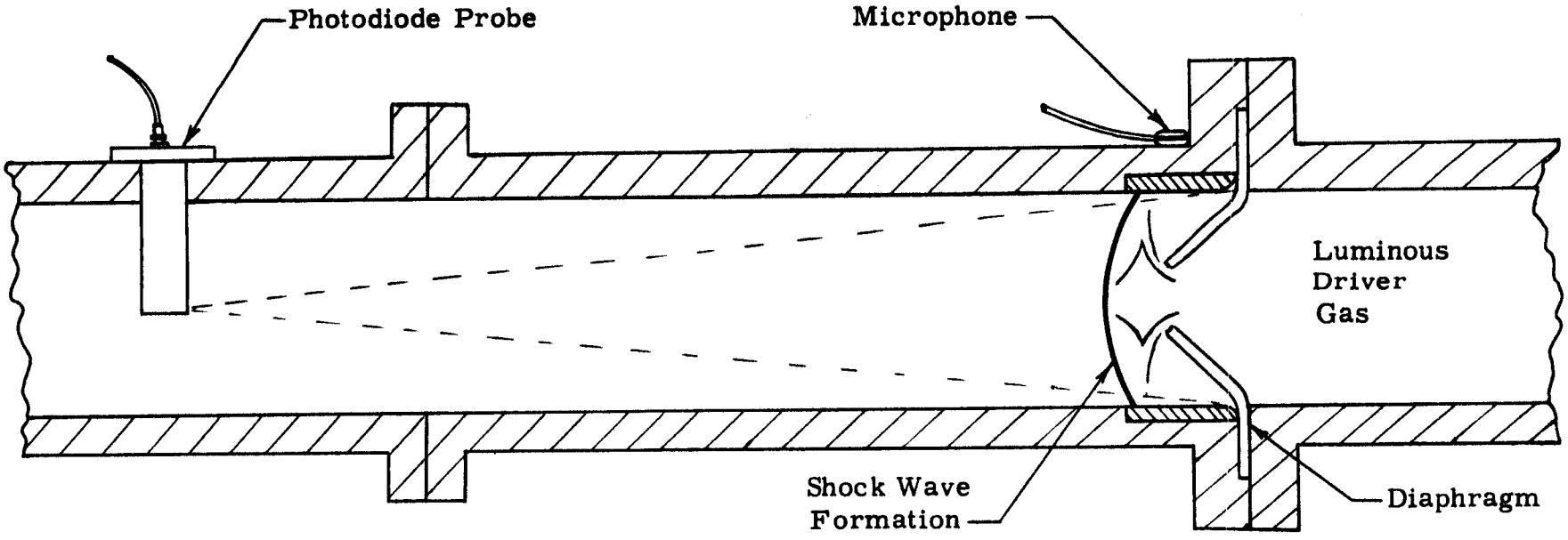

FIG. 1. GENERAL EXPERIMENTAL ARRANGEMENT FOR MEASUREMENT OF DIAPHRAGM OPENING-TIMES

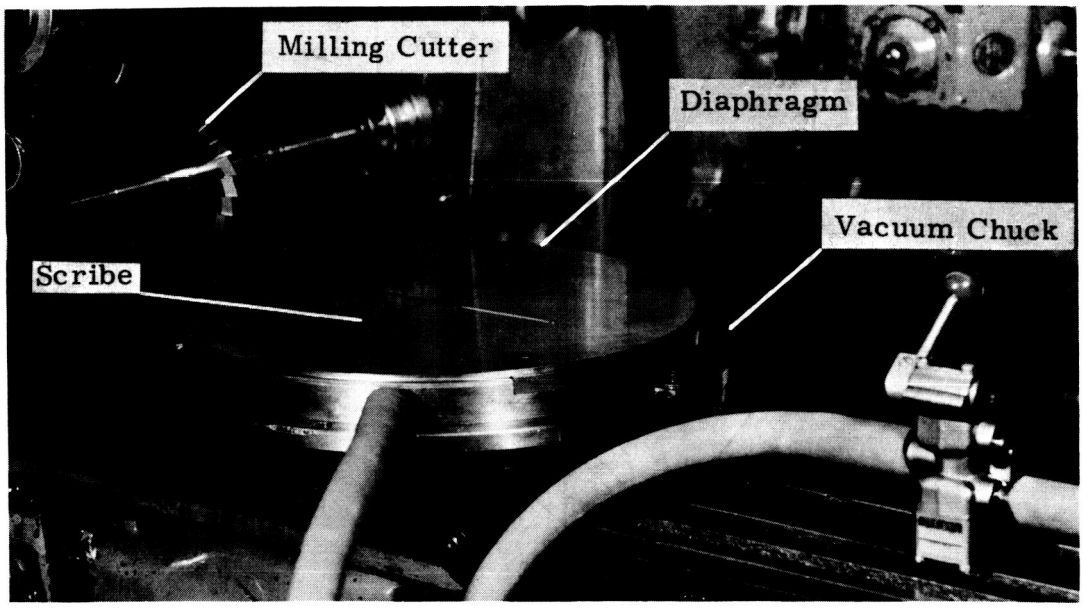

(a) Diaphragm Scribing Technique

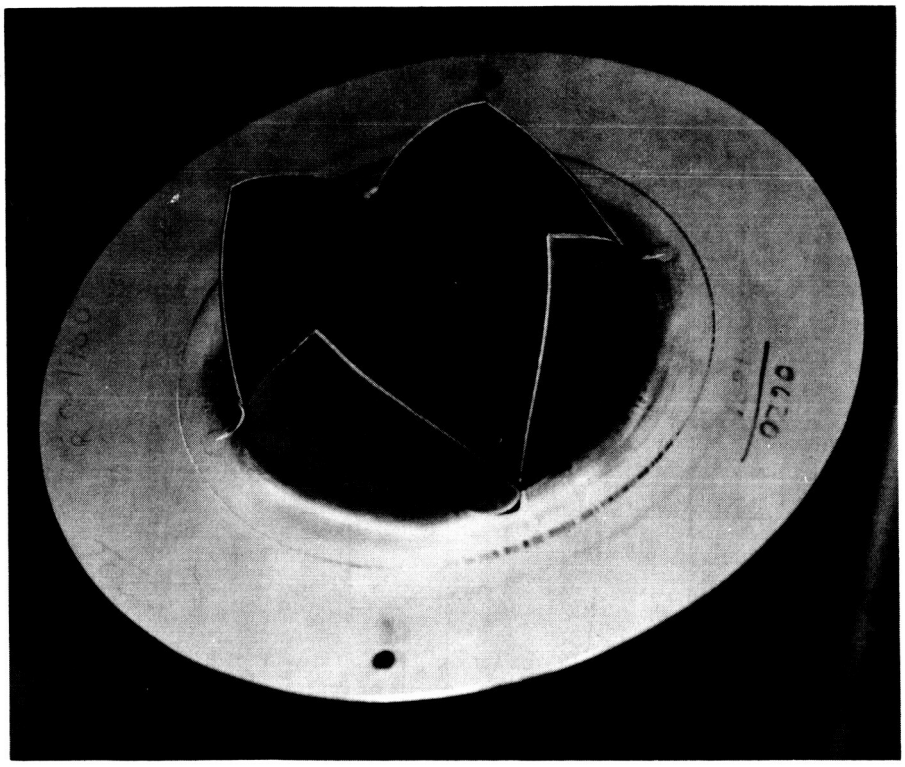

(b) Ruptured Diaphragm

FIG. 2. SHOCK TUBE DIAPHRAGMS

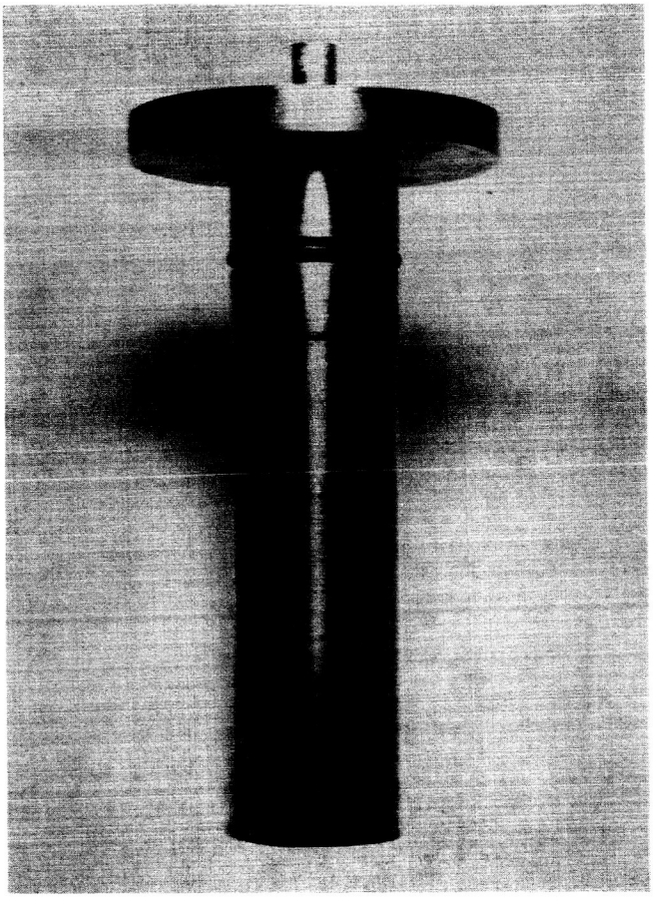

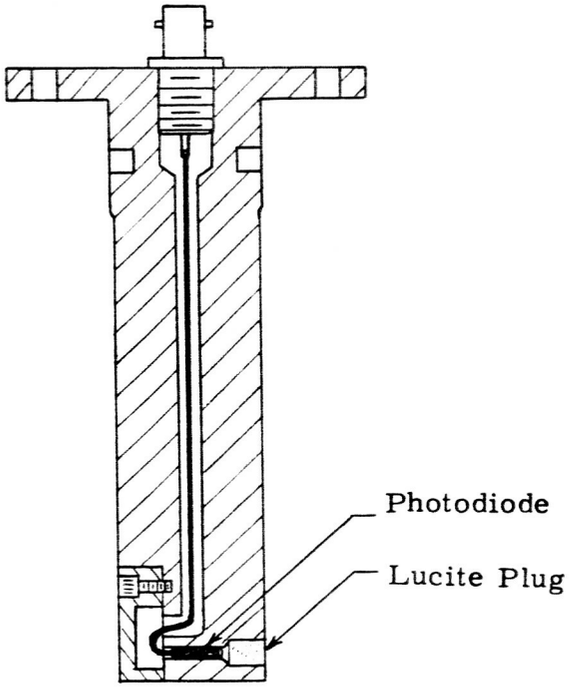

FIG. 3. PHOTODIODE PROBE

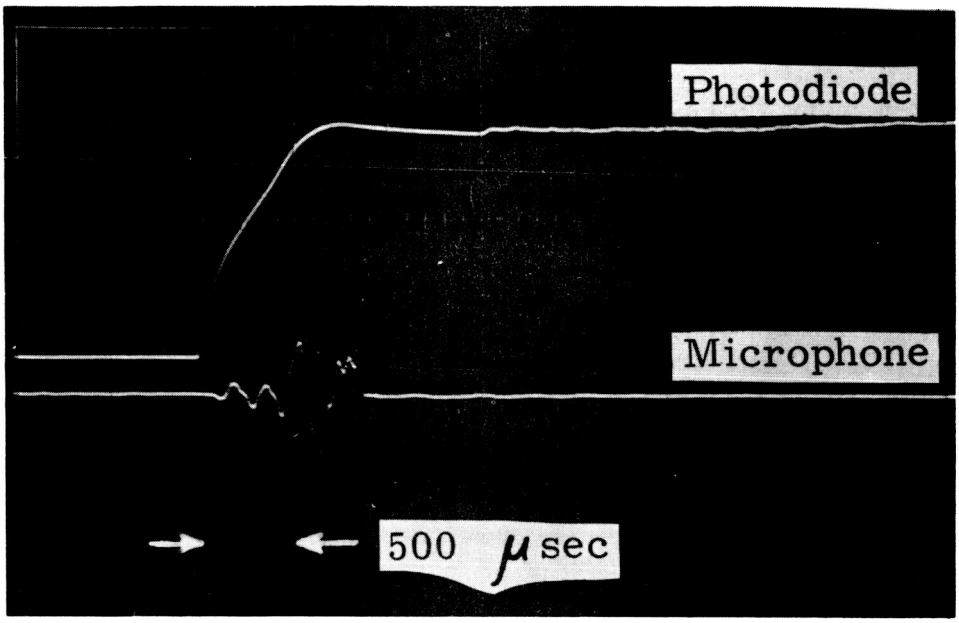

(a) Photodiode Facing Upstream Towards Diaphragm

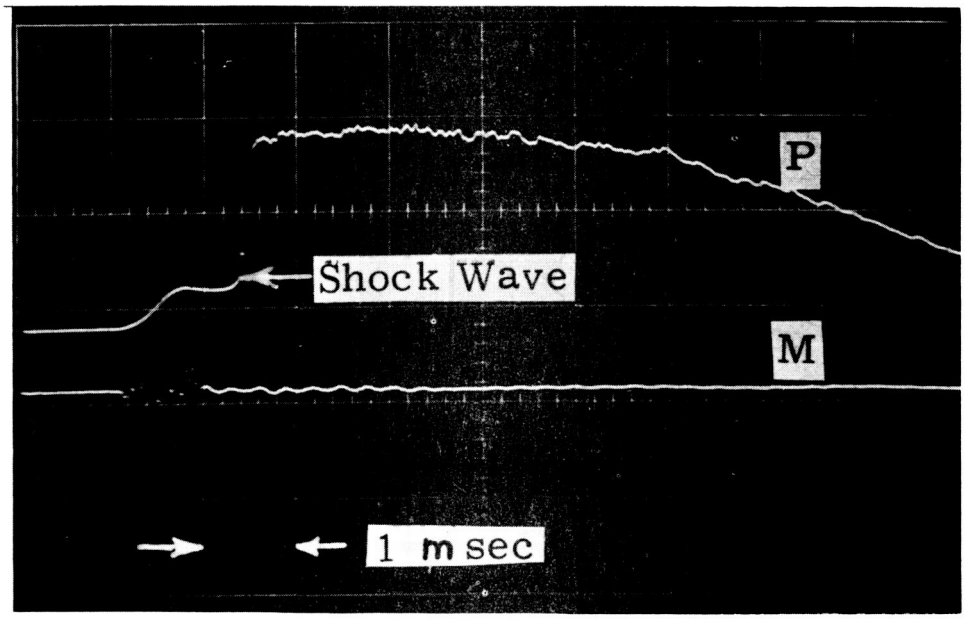

(b) Photodiode Facing Transverse to Flow Direction

FIG. 4. MEASUREMENTS OF DIAPHRAGM OPENING-TIMES

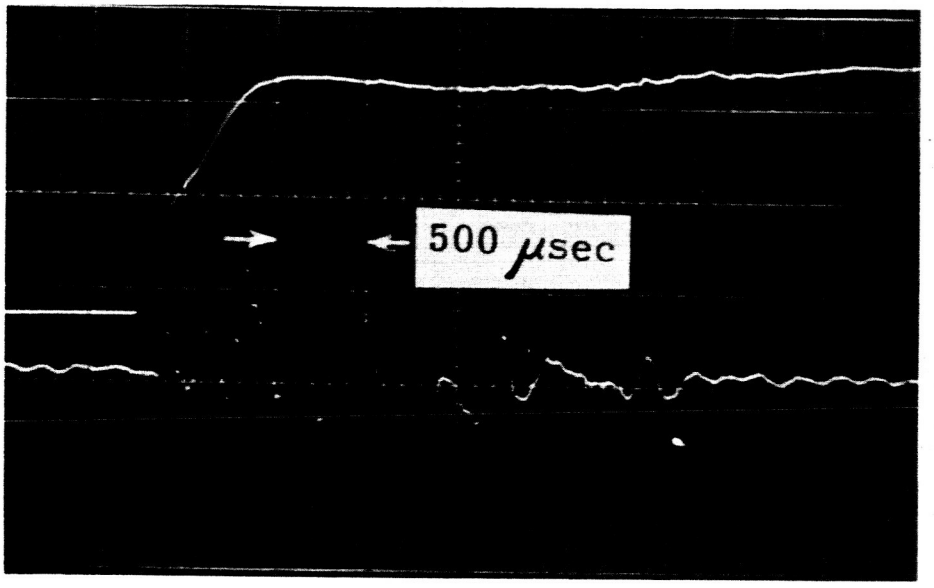

(a) Normal Photodiode Result

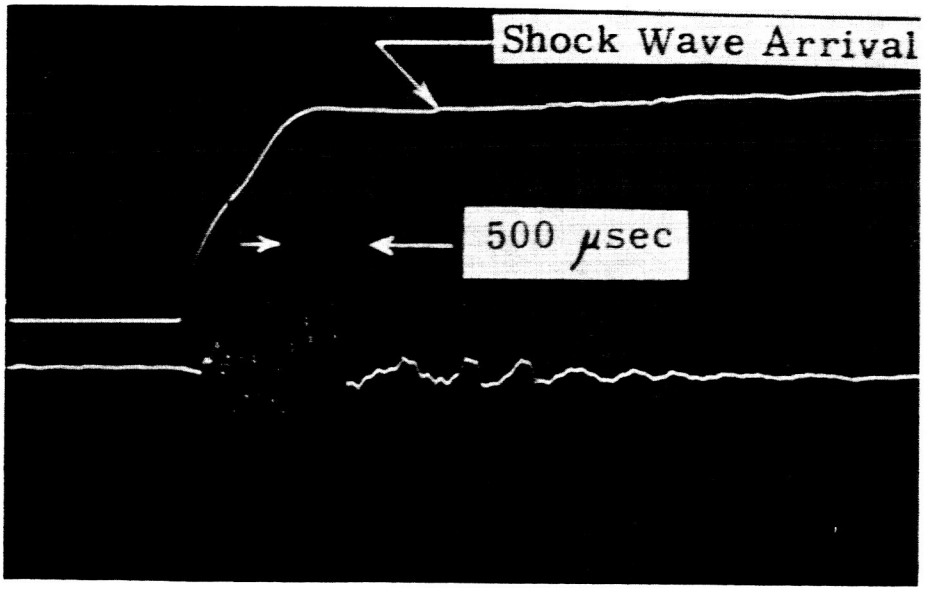

(b) Collimated Photodiode Result

FIG. 5. COMPARISON OF NORMAL AND COLLIMATED PHOTODIODE MEASUREMENTS

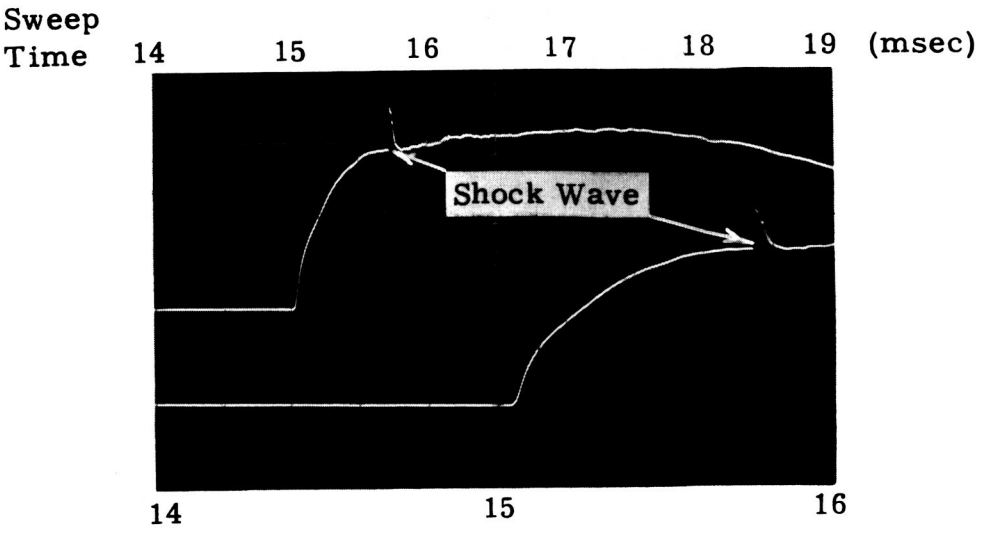

Photodiode

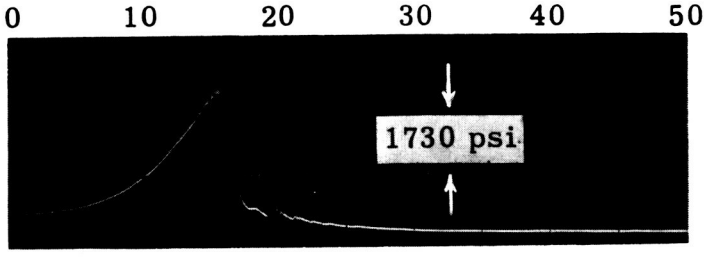

Combustion-driver Pressure

FIG. 6. CORRELATION BETWEEN PHOTODIODE RESPONSE AND COMBUSTION-DRIVER PRESSURE RISE

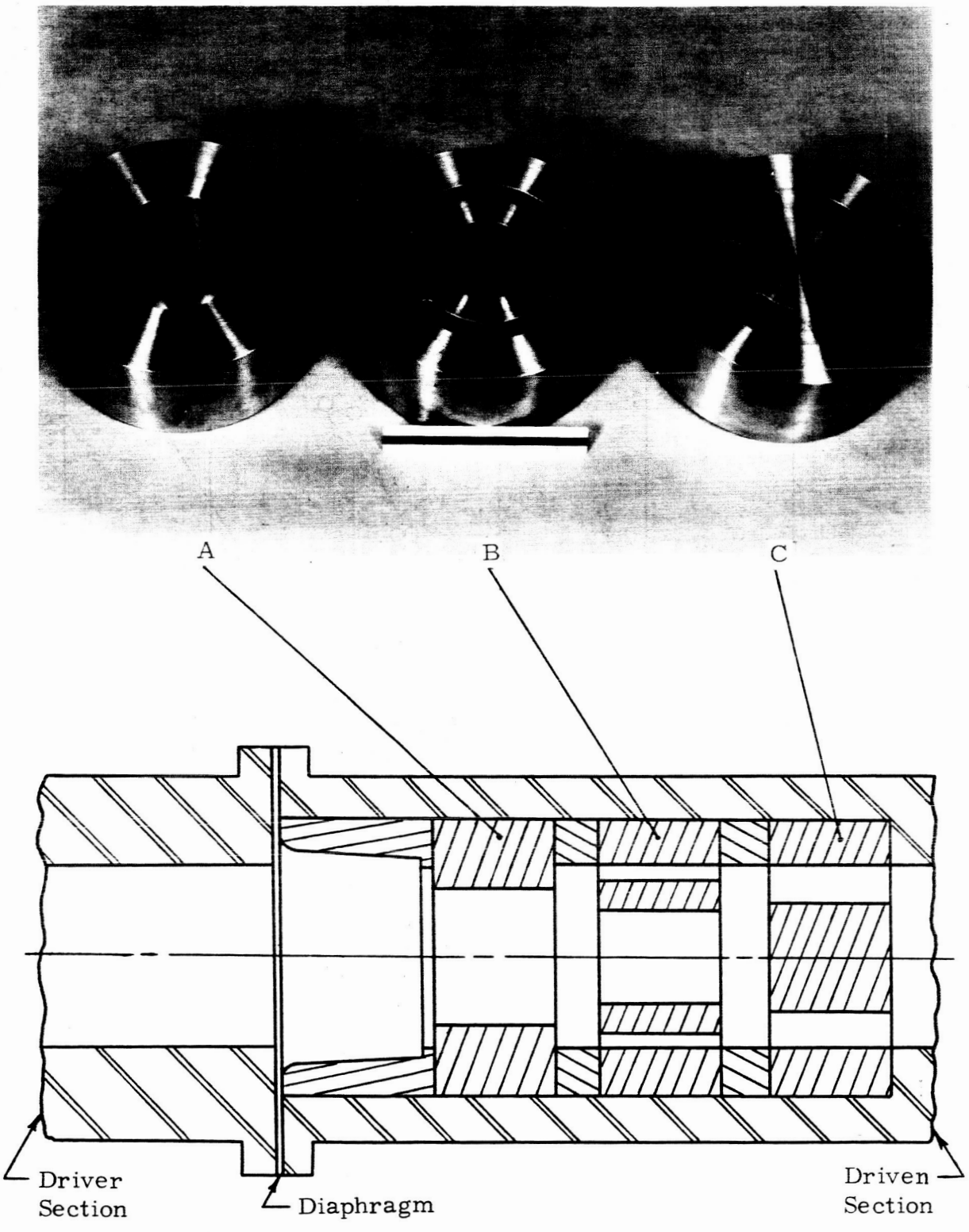

FIG. 7 DIAPHRAGM PARTICLE TRAPS

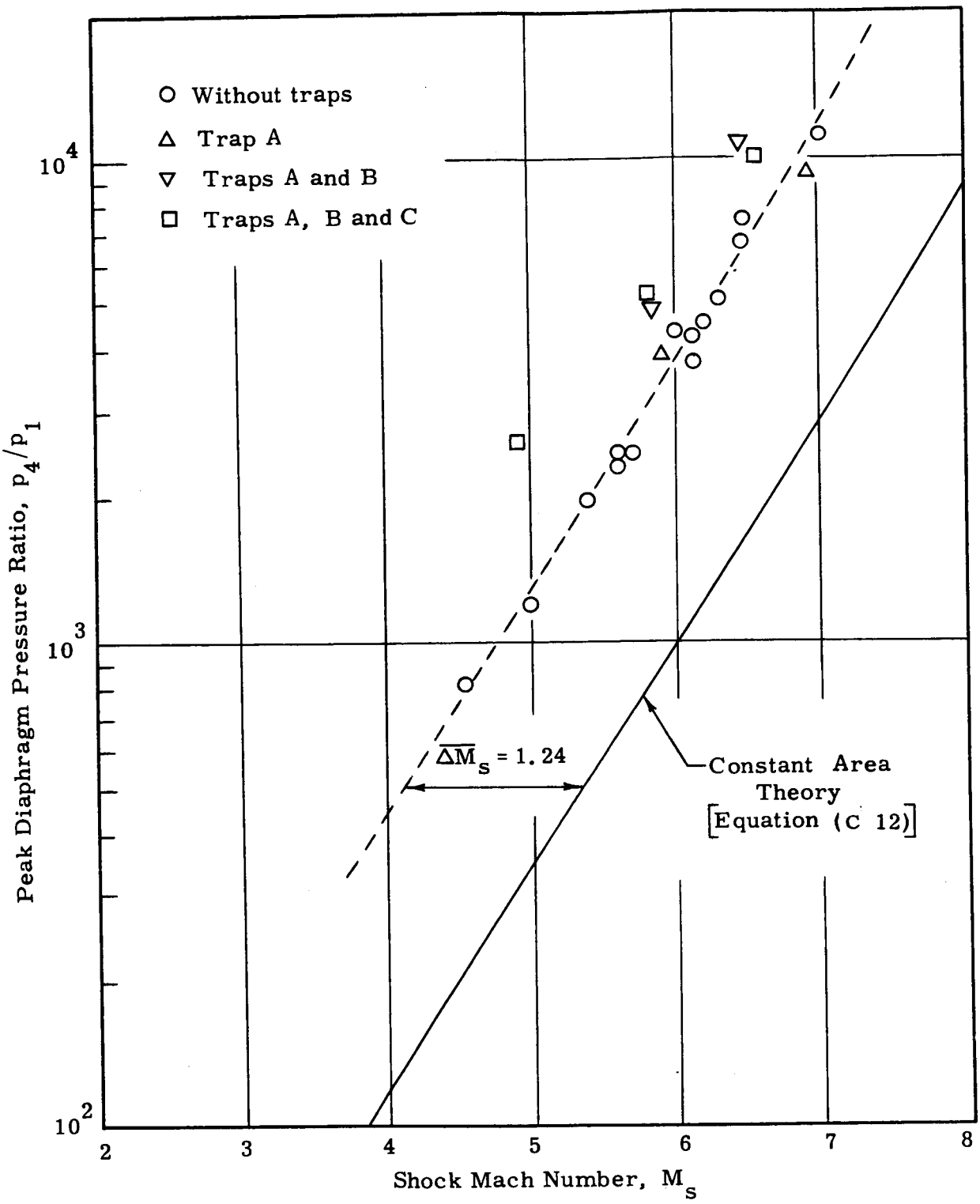

FIG. 8. SHOCK TUBE PERFORMANCE WITH AND WITHOUT PARTICLE TRAPS FOR COMBUSTION DRIVER(STOICH. $H_2 - O_2$; 75% Ar) AND DRIVEN AIR

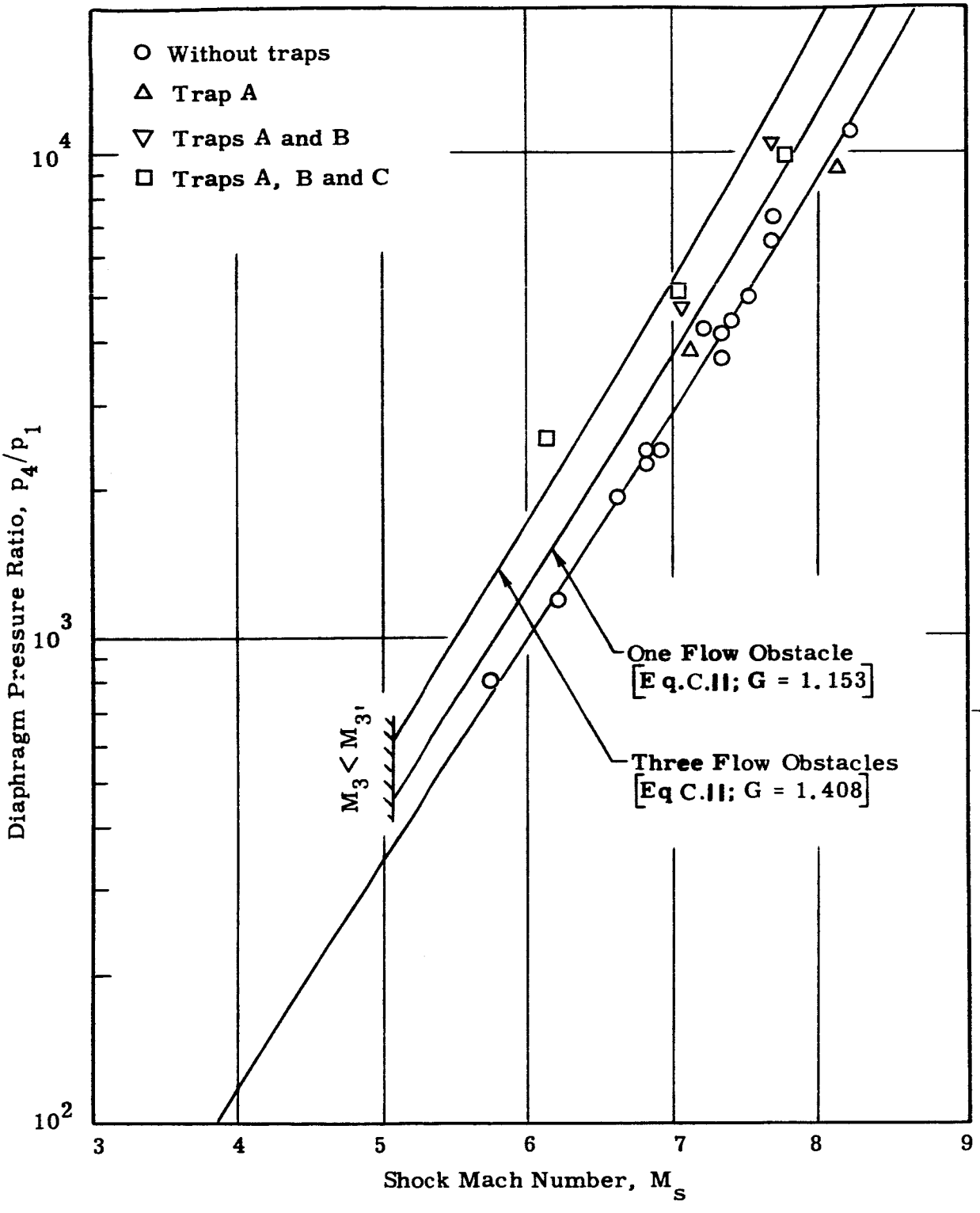

FIG. 9. COMPARISON OF ADJUSTED EXPERIMENTAL DATA WITH THEORETICAL RESULTS FOR ONE AND THREE FLOW OBSTACLES

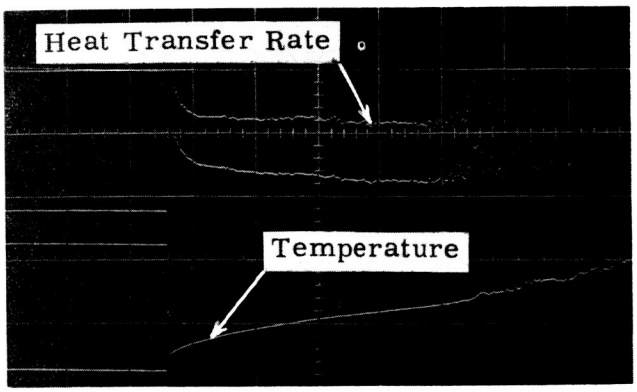

(a) p_1 = 20 mmHg

M_s = 6.3

No particle traps

(b) p_1 = 20 mmHg

M_s = 5.8

Three particle traps

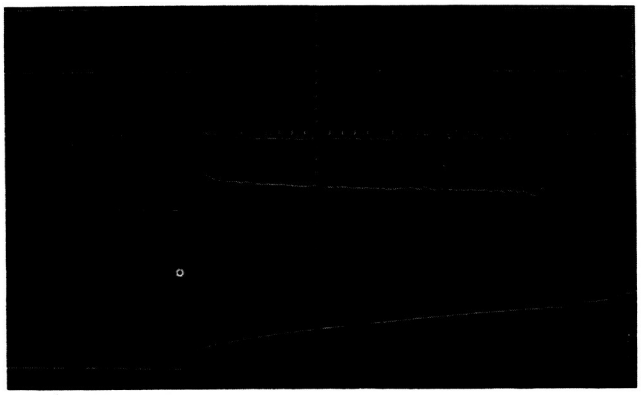

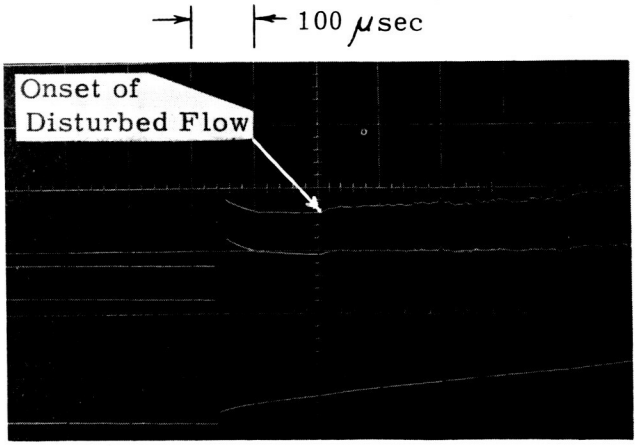

(c) p_1 = 40 mmHg

M_s = 4.9

Three particle traps

FIG. 10. RESULTS OF HEAT TRANSFER RATE MEASUREMENTS

APPENDIX A

Simplified Derivation of Diaphragm Opening-Time

The problem of diaphragm rupture is quite complicated as a result of the complex flow pattern around the diaphragm petals during rupture as well as the dynamic stress-strain processes inside the diaphragm itself. In order to simplify the problem the following assumptions are made:

(i) The shock tube cross-section at the diaphragm station is assumed to be square with an area equivalent to the actual circular cross-section area.

(ii) The diaphragm ruptures instantaneously without any prior deformation.

(iii) Four identical triangular petals are formed upon rupture.

(iv) The force acting on each petal is a linear function of the opening area, varying from a maximum initial value to zero when the diaphragm is fully open. At any instant the force is assumed to be uniform over the petal surface and acting at its centroid.

(v) The moment due to bending stresses in the petal is assumed as being constant during the rupture process.

The equation of motion for the diaphragm petal (see Fig. A. 1) may be written as

$$I \frac{d^2\theta}{dt^2} = \frac{Fb}{6} - M_\sigma \qquad (A.1)$$

where

I = moment of inertia of diaphragm petal about its base line

F = force acting on petal

M_σ = moment due to bending stresses in petal

For the triangular diaphragm petal the moment of inertia about its base is

$$I = \frac{\rho_d b^4 \tau}{96} \qquad (A.2)$$

and the force acting on the petal may be written as

$$F = \frac{p_4 b^2 \cos\theta}{4} \qquad (A.3)$$

where p_4 is the peak combustion-driver pressure.

Assuming a uniform stress distribution in the petal, the moment due to the bending stresses may be written as

$$M_\sigma = \frac{\sigma b \tau^2}{4} \qquad (A.4)$$

Substituting Eqs. (A.2), (A.3) and (A.4) into Eq. (A.1) yields the following result

$$\frac{d^2\theta}{dt^2} = \frac{4 p_4 \cos\theta}{\rho_d b \tau} \left[1 - \frac{6}{\cos\theta} \frac{\tau^2}{b^2} \frac{\sigma}{p_4}\right] \qquad (A.5)$$

Since $\tau \ll b$ and assuming that $\sigma/p_4 \sim 1$, the second term in the bracket above may be neglected as a first approximation. The resulting relation may then be integrated twice to obtain

$$t = 4.73 \left[\frac{\rho_d b \tau}{p_4}\right]^{\frac{1}{2}} \times 10^4 \quad (\mu\text{sec.}) \qquad (A.6)$$

where the constants of integration are evaluated using the initial conditions $\theta = 0$ and $\frac{d\theta}{dt} = 0$ at $t = 0$.

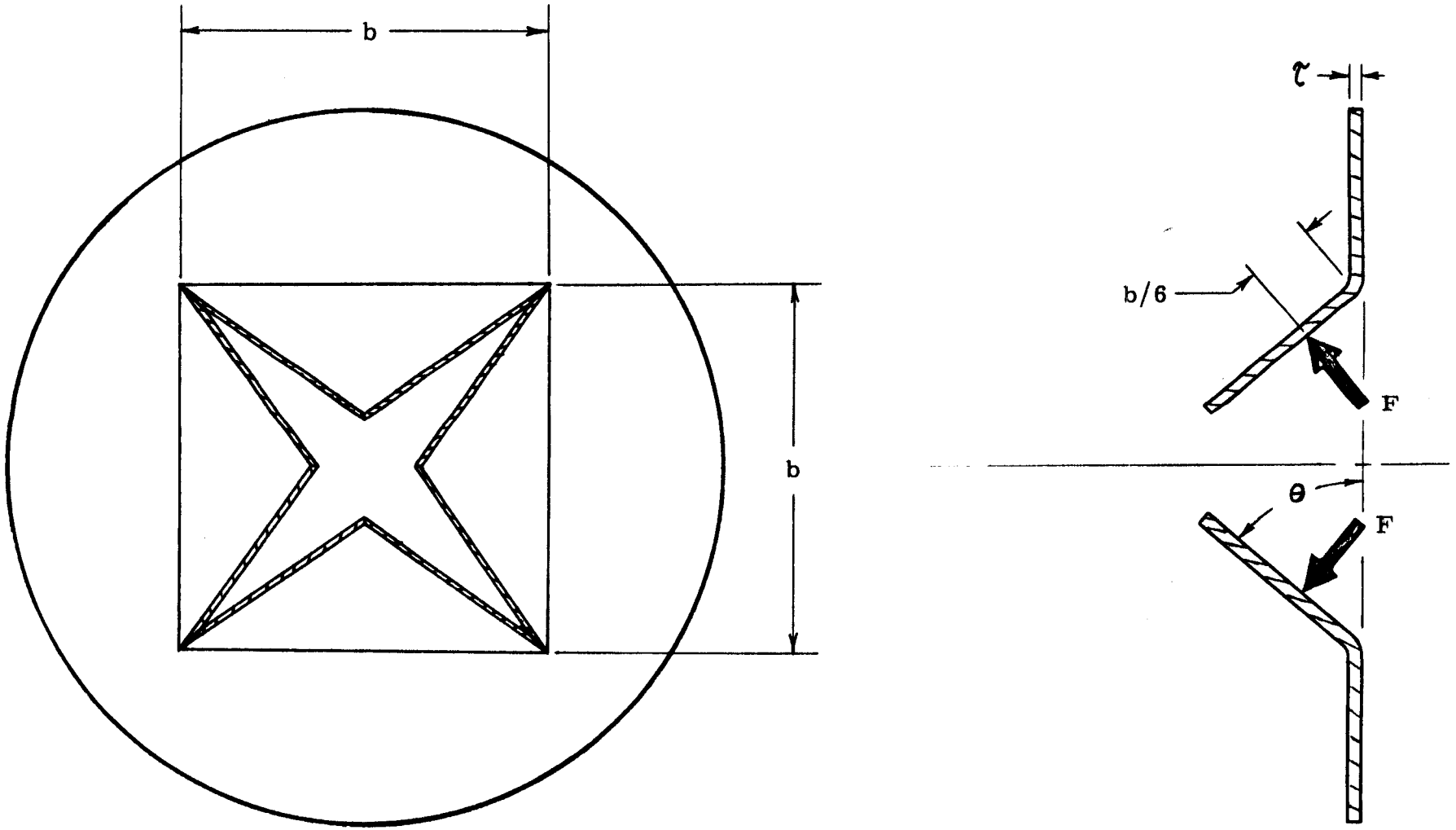

FIG. A.1. SCHEMATIC OF THEORETICAL MODEL FOR DIAPHRAGM RUPTURE

APPENDIX B

Design of Particle Trap System

The basic requirements which were considered in the design of the set of particle traps shown in Fig. 7 were (1) to provide maximum blockage to solid diaphragm particles and (2) to try to minimize the overall disturbance to the shock tube flow as much as possible.

In order to satisfy the first criterion, it was necessary to start with a trap system that was optically tight. However, in light of the second criterion, it seemed logical that, in order to reduce the disturbances in the flow, the trapping of particles should be made through a series of "partial traps", or flow obstacles, rather than in a sudden and more-nearly total blockage of the flow. These flow obstacles would be separated from each other as much as possible within the space available for their location in the shock tube. Although the entire set of traps may form an optically-tight system, the provision of space between adjacent traps for flow expansion meant there may still be some possibility for particles to pass through the traps if their trajectories conformed to flow streamlines. In other words, a certain amount of trap overlapping might be required in order to achieve complete (or nearly complete) particle trapping.

In order to gain some insight a simplified analysis was made of the motion of solid particles in a uniform, irrotational flow passing through a series of flow obstacles such as for the present traps. The basic equation of particle motion may be expressed as

$$\frac{dV}{dt} = \frac{c_D \rho S}{2m} (U - V)^2 \qquad \text{(B. 1)}$$

where

V = particle velocity

U = flow velocity

c_D = particle drag coefficient

m = particle mass

ρ = flow density

S = particle reference area

In Eq. (B. 1) only aerodynamic forces are considered since they are generally several orders of magnitude greater than gravitational forces. The particle drag coefficient c_D is, in general, a function of Reynolds number and Mach number. However, since the particle velocity relative to that of the flow is always subsonic, the influence of Mach number on c_D was assumed to be negligible. For the sake of simplicity, the dependence of c_D on Reynolds number was also assumed to be invariant over the range of flow conditions of interest.

Referring to the coordinate system shown in Fig. B. 1, it is convenient to introduce the following nondimensional parameters

$$x' = \frac{x}{L}; \quad y' = \frac{y}{L}; \quad t' = \frac{t}{T}$$

$$u' = \frac{V_x}{U}; \quad v' = \frac{V_y}{U} \tag{B. 2}$$

where

$$L = \frac{2m}{c_D \rho S} \quad \text{and} \quad T = \frac{2m}{c_D \rho US}$$

One may then rewrite Eq. (B. 1) as

$$\frac{du'}{dt'} = (\cos\alpha - u')^2 \tag{B. 3}$$

for the x - direction and

$$\frac{dv'}{dt'} = (\sin\alpha - v')^2 \tag{B. 4}$$

for the y - direction.

The initial conditions which may be used to solve Eqs. (B. 3) and (B. 4) are as follows

$$t' = 0 \begin{cases} x' = y' = 0 \\ u' = u'_o = \dfrac{V_o}{U} \\ v' = 0 \end{cases}$$

The solutions for these two equations are found to be

$$u' = \cos\alpha - \frac{1}{t' + \frac{1}{\cos\alpha - u_o}} \qquad \text{(B. 5)}$$

and

$$v' = \sin\alpha - \frac{1}{t' + \frac{1}{\sin\alpha}} \qquad \text{(B. 6)}$$

Since $u' = \frac{dx'}{dt'}$ and $v' = \frac{dy'}{dt'}$,

one may then integrate the above relations to obtain

$$x' = t'\cos\alpha - \ln\left[1 + t'(\cos\alpha - u_o)\right] \qquad \text{(B. 7)}$$

and

$$y' = t'\sin\alpha - \ln\left[1 + t'\sin\alpha\right] \qquad \text{(B. 8)}$$

These resulting expressions provide a parametric relation between x' and y'.

Calculations based on arbitrary values of α and u'_o have been made and the results are given in Fig. B. 2. As may be seen the amount of particle deflection downstream of the first trap decreases as the initial particle velocity u_o at the exit of the first trap increases. From Fig. B. 3, for fixed values of u'_o and α, one may then obtain the values for nondimensional particle deflection and velocity at any given distance downstream of the first trap--in particular, the distance corresponding to the location of the front surface of the second trap.

For the special case where the particle velocity and flow velocity are parallel (i.e., inside the first trap) one obtains the following result for particle velocity

$$u' = \frac{t'}{1 + t'} \qquad \text{(B. 9)}$$

In deriving Eq. (B. 9) it was assumed that all particles originated at the diaphragm and thus were motionless at $t = 0$.

Integrating Eq. (B. 9) one obtains the following result

$$x' = t' - \ln\left[(1 + t')\right] \qquad \text{(B. 10)}$$

Combining Eqs. (B. 9) and (B. 10) one then gets an explicit relation between u' and x which is given as

$$x' = \frac{u'}{1 - u'} + \ln \left[(1 - u') \right] \qquad \text{(B. 11)}$$

From Eq. (B. 11) it is possible to determine the particle velocity at the exit of the first trap. A plot of Eq. (B. 11) is given in Fig. B. 3.

Making use of the methods outlined above along with those discussed in Appendix C, an approximate analysis of the motion of diaphragm particles was carried out under the following assumptions:

(i) Flow inside the region, or core, defined by the diameter d_2 (see Fig. B. 4) is assumed to be undisturbed while the flow outside this region is outwardly deflected.

(ii) Flow streamlines of the deflected flow are approximated by straight lines having a "mean" deflection angle α which is based simply on existing geometry.

(iii) Flow velocity and density in the region between Traps A and B (see Figs. 7 and B. 4) are assumed to be constant and equal to their values at the exit area of the first trap.

For purposes of calculation, particle diameters of . 01 mm., . 1 mm., and 1 mm., were used. These particles were assumed to have a mass density of 7. 8 kg/m^3 corresponding to that of the diaphragm material which was stainless steel. The drag coefficient for these particles was taken to be about 0. 4 (Ref. 11).

The calculated values obtained for particle deflection in the region between the first two traps were . 15 in., . 04 in., and . 025 in. for the . 01 mm., . 1 mm., and 1 mm. diameter particles, respectively. Since the second trap surface overlapped the first by an amount of . 25 in. (see Fig. B. 4) all of the particles considered would, hypothetically, strike the surface of the second trap.

As for the particles passing through the open center portion of the second trap, it was concluded that their deflection in the region between the latter two traps would be less than that calculated above since they would have achieved a higher velocity (and hence momentum) in the downstream direction. Since the same amount of overlapping (0. 25 in.) existed, these particles would all strike the surface of the third trap.

It is realized that the foregoing analysis is quite approximate in nature. However, it was felt that since these considerations were used in the design of the particle trap system it was worthwhile to mention them here.

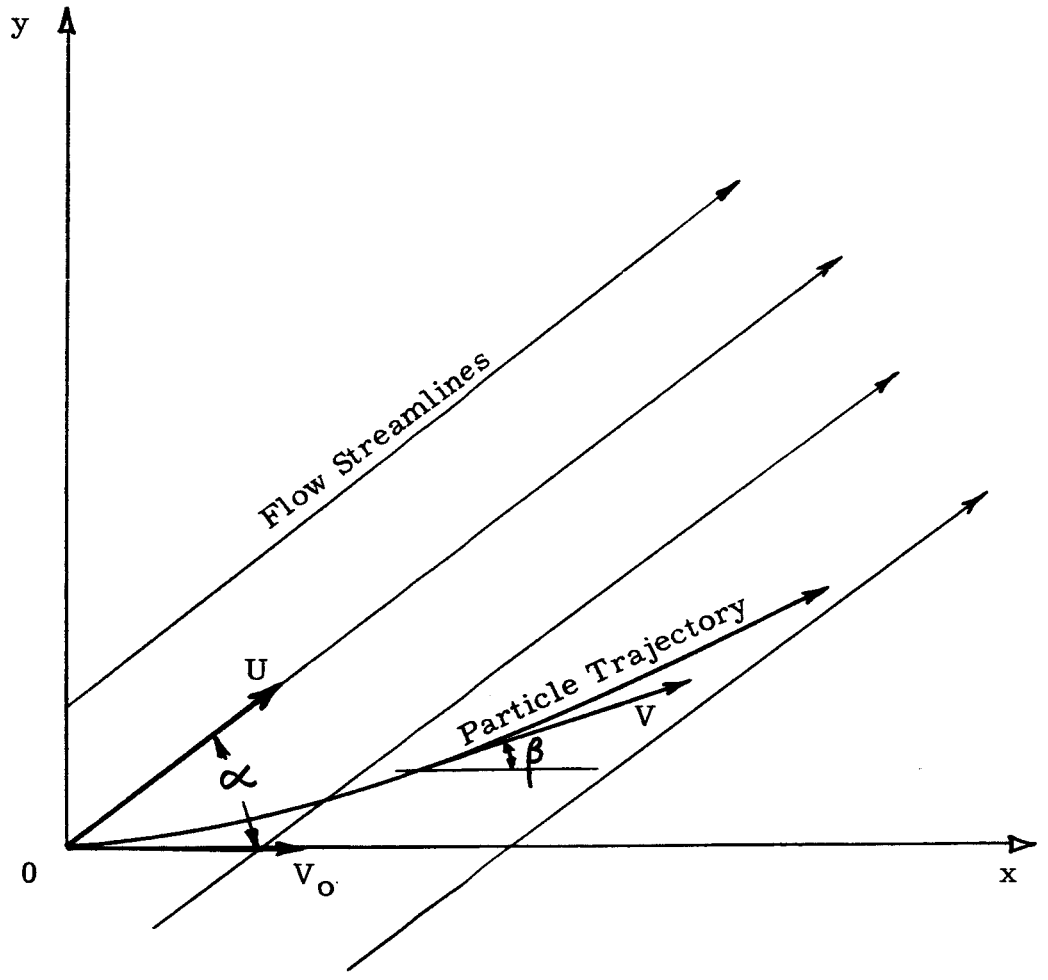

FIG. B. 1 PHYSICAL COORDINATE SYSTEM FOR PARTICLE MOTION IN DEFLECTED FLOW REGION.

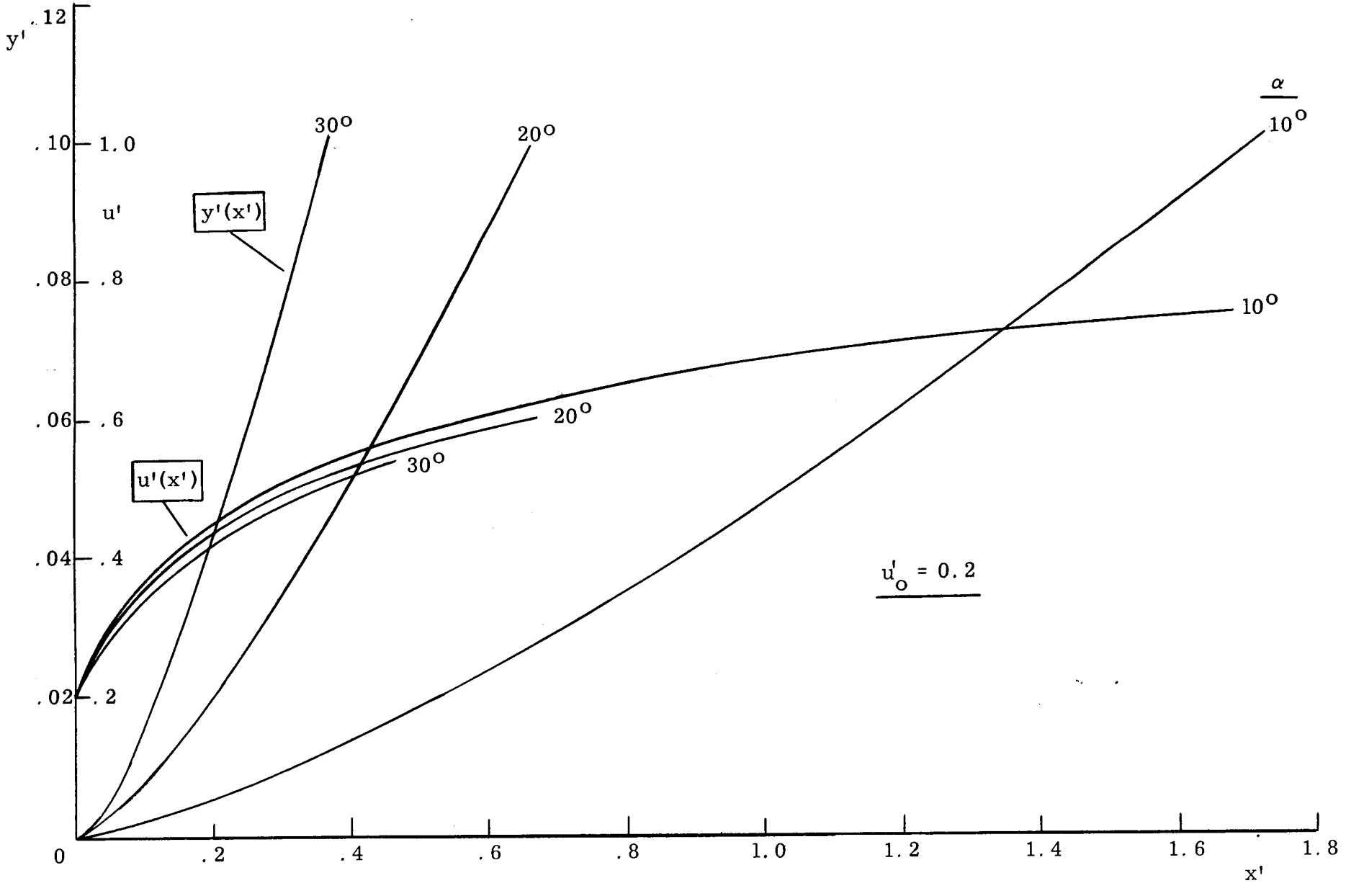

FIG. B.2 DIMENSIONLESS PARTICLE VELOCITY AND DEFLECTION IN DEFLECTED FLOW REGION (con't.)

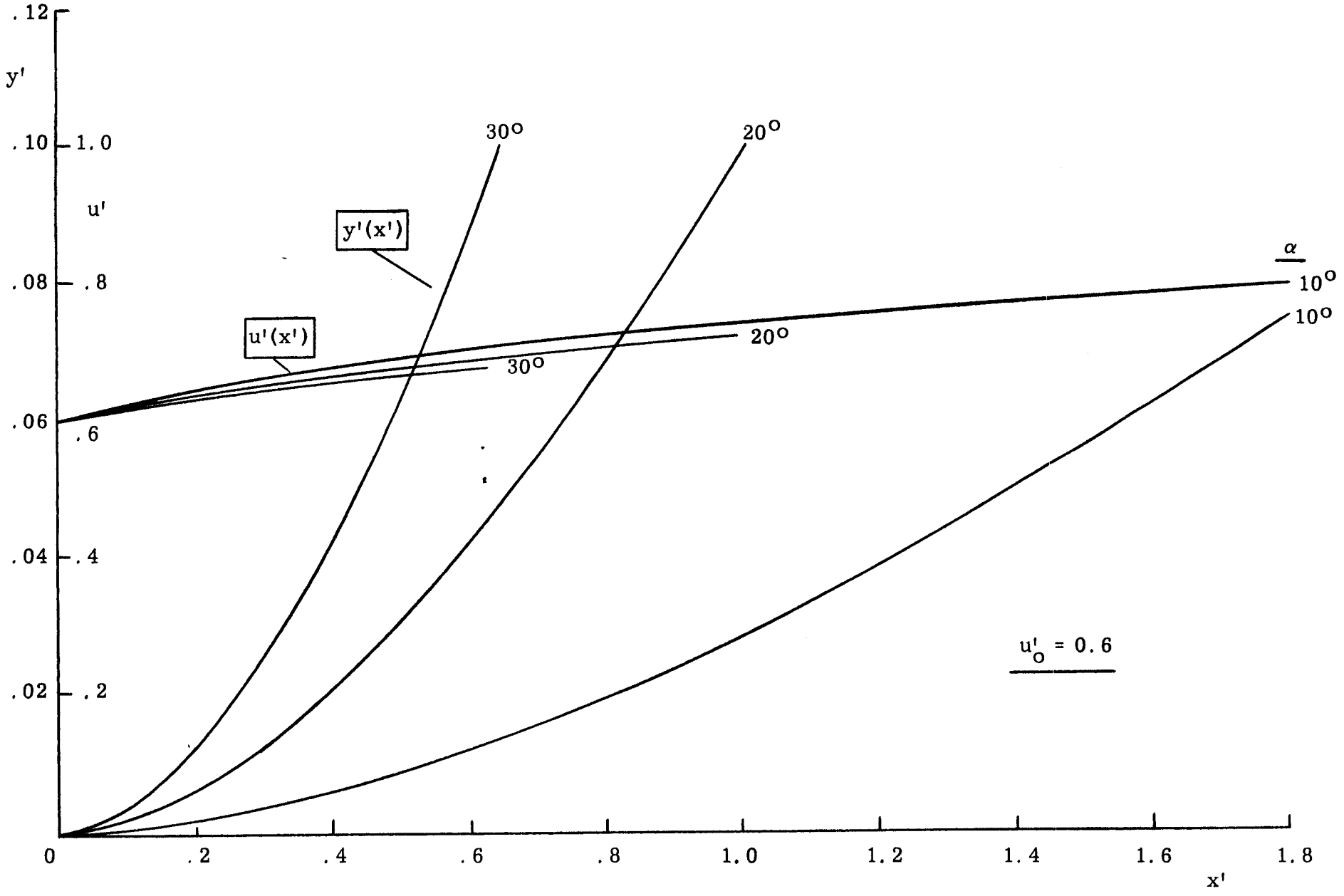
.12
y'
.10
1.0
u'
.08
.8
.06
.6
.04
.4
.02
.2
0
.2
.4
.6
.8
1.0
1.2
1.4
1.6
1.8
x'
30°
20°
y'(x')
u'(x')
α
10°
20°
30°
10°
u'o = 0.6

FIG. B.2 (con't)

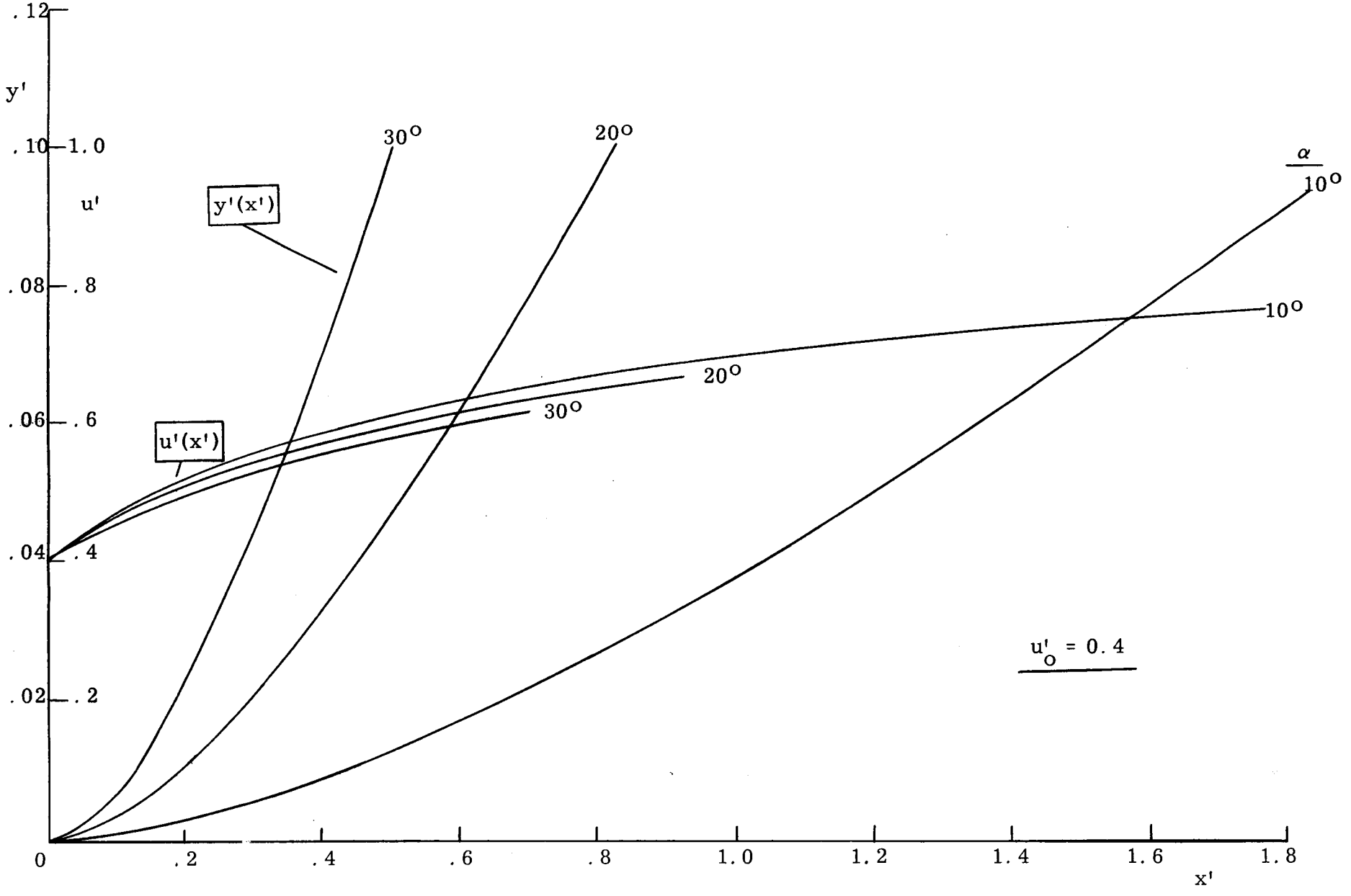
.12
y'
.10
1.0
u'
30°
20°
α
10°
y'(x')
.08
.8
10°
20°
.06
.6
30°
u'(x')
.04
.4
u'o = 0.4
.02
.2
0
.2
.4
.6
.8
1.0
1.2
1.4
1.6
1.8
x'

FIG. B.2 (con't)

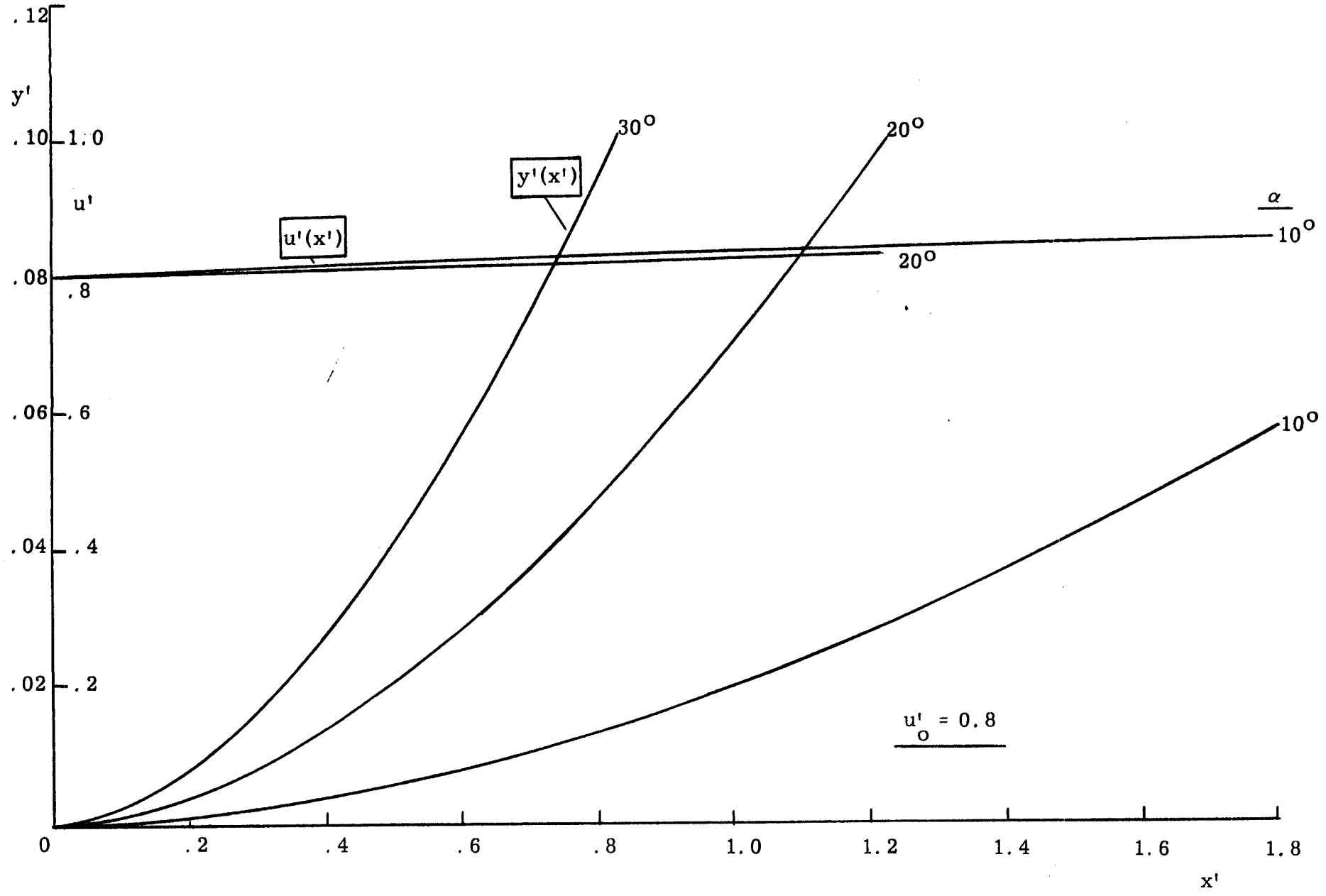
.12
y'
.10
1.0
u'
.08
.8
.06
.6
.04
.4
.02
.2
0
.2
.4
.6
.8
1.0
1.2
1.4
1.6
1.8
x'
y'(x')
u'(x')
30°
20°
10°
α
20°
10°
u'o = 0.8

FIG. B.2 (con't.)

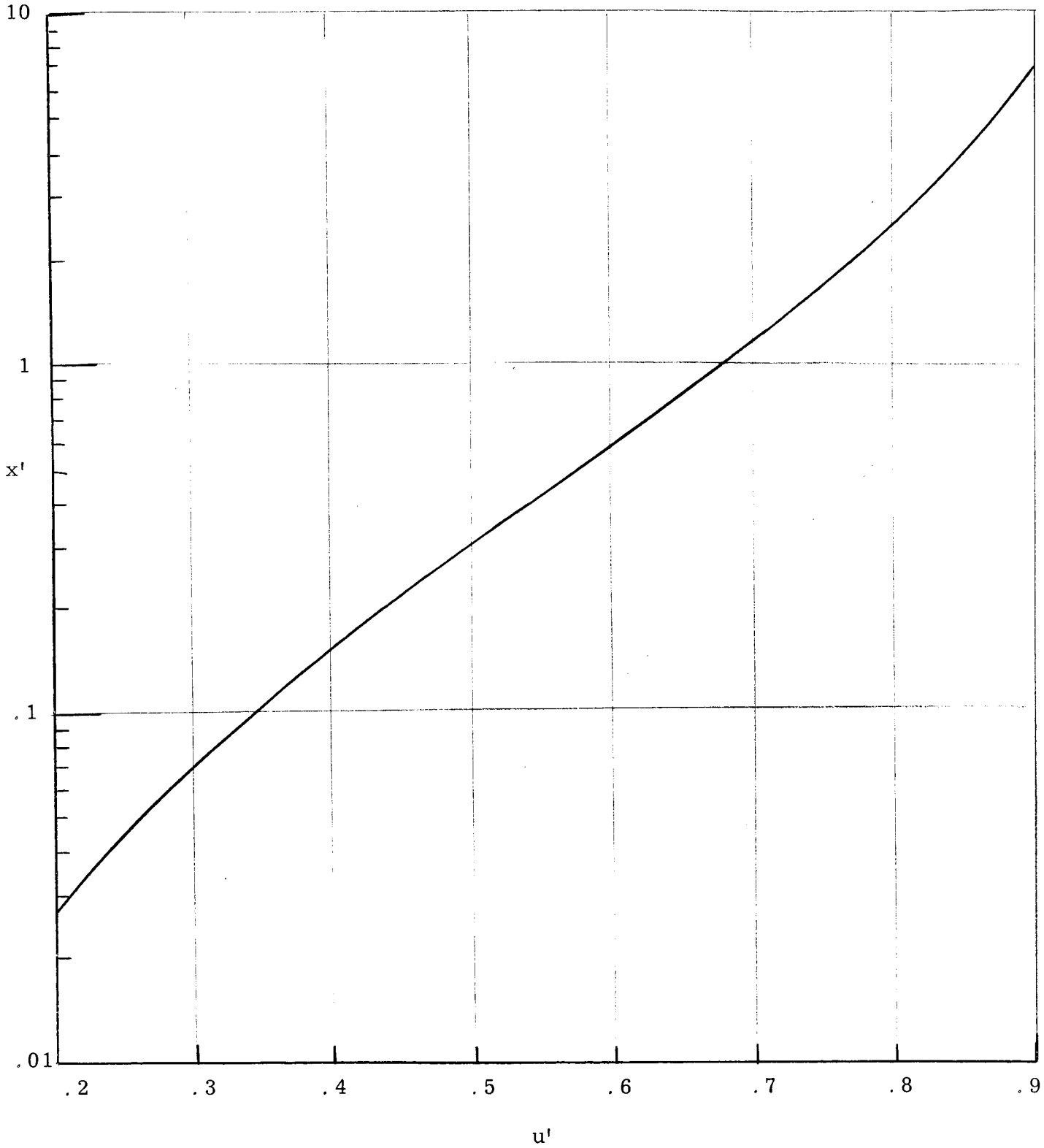

FIG. B. 3 DIMENSIONLESS PARTICLE VELOCITY IN UNDISTURBED FLOW REGION ($\alpha = 0^{o}$)

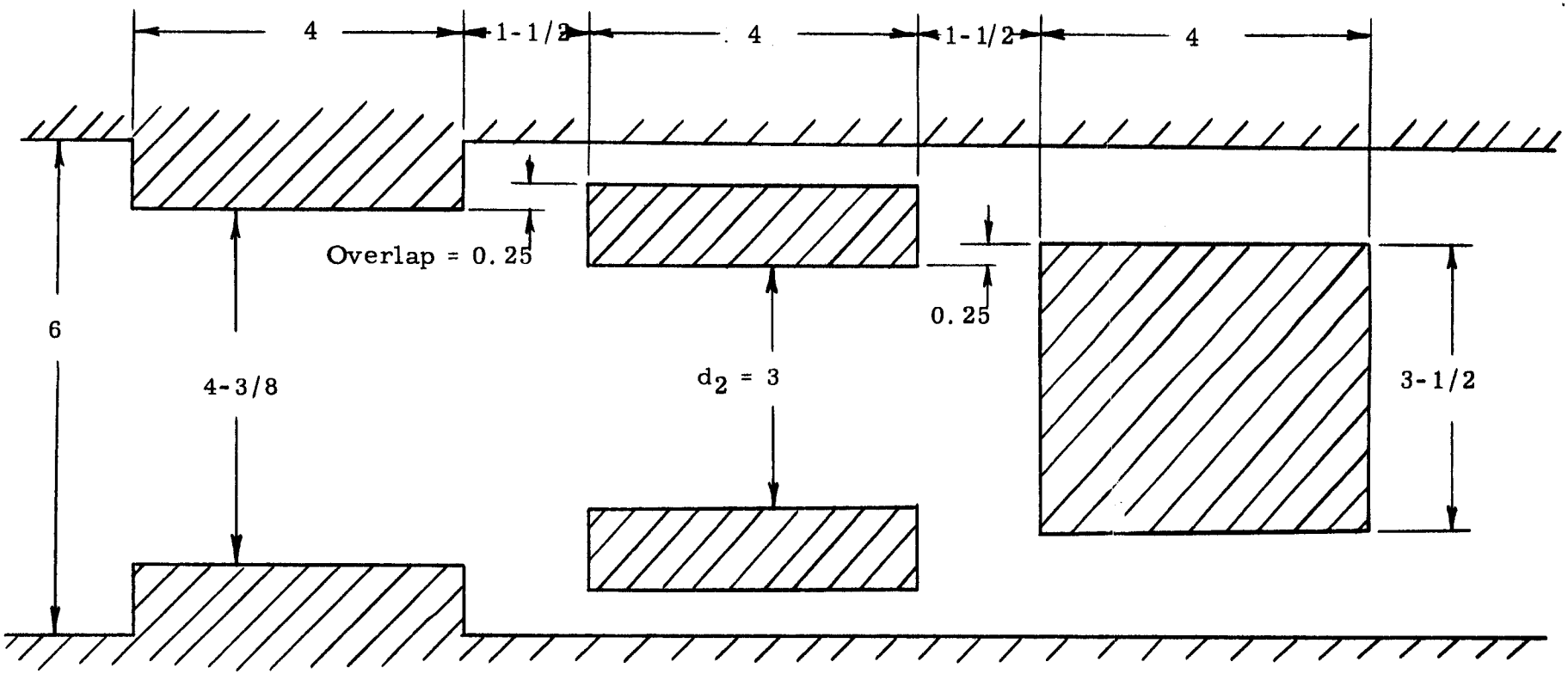

FIG. B.4 SCHEMATIC OF PARTICLE TRAP SYSTEM SHOWING BASIC DIMENSIONS

APPENDIX C

Calculation of Shock Tube Performance with Particle Traps

In order to more easily examine the influence of a flow obstacle, such as a particle trap, on the performance of a shock tube it is convenient to make certain simplifying assumptions (Refs. 5-9):

(i) The flow obstacle is assumed to be located at the diaphragm station (i.e., at $x = 0$).

(ii) The flow past the obstacle is assumed to be a steady, isentropic expansion from subsonic to supersonic speed.

For the present we will consider only the strong shock wave case where it is assumed (Ref. 5) that an unsteady, left-running rarefaction wave $\overleftarrow{R}_2$ (see Fig. C.1) occurs between the flow obstacle and the contact surface $\overleftarrow{C}$. The wave diagram for such a case is given in Fig. C.2.

Following the simple procedure outlined in Ref. 5 (see also Refs. 6 and 7), the overall pressure ratio across the diaphragm may be expressed as

$$\frac{p_4}{p_1} = \frac{p_4}{p_{4'}} \cdot \frac{p_{4'}}{p_{3'}} \cdot \frac{p_{3'}}{p_3} \cdot \frac{p_3}{p_2} \cdot \frac{p_2}{p_1} \tag{C.1}$$

The pressure ratio across the unsteady rarefaction wave $\overleftarrow{R}_1$ may be written as

$$\frac{p_4}{p_{4'}} = \left[1 + \beta M_{4'}\right]^{\alpha/\beta} \tag{C.2}$$

where

$$\beta = \frac{\gamma_4 - 1}{2}$$

The pressure ratio across the flow obstacle may be written as (see assumption (ii))

$$\frac{p_{4'}}{p_{3'}} = \frac{A_1}{A_4} \frac{M_{3'}}{M_{4'}} \left[\frac{1 + \beta M_{3'}^2}{1 + \beta M_{4'}^2}\right]^{\frac{1}{2}} \tag{C.3}$$

Across the unsteady rarefaction wave $\overleftarrow{R}_2$ the pressure ratio is given as

$$\frac{p_{3'}}{p_3} = \left[\frac{1 + \beta M_3}{1 + \beta M_{3'}}\right]^{\gamma_4/\beta} \qquad (C.4)$$

Finally, across the contact surface $p_3 = p_2$ and from one-dimensional shock tube theory (Ref. 10) one gets

$$\frac{p_2}{p_1} = 1 + \frac{2\gamma_1}{\gamma_1 + 1}(M_s^2 - 1) \qquad (C.5)$$

For air as the driven gas, Eq. (C.5) becomes

$$\frac{p_2}{p_1} = \frac{7 M_s^2 - 1}{6} \qquad (C.6)$$

Combining Eqs. (C.2), (C.3), (C.4) and (C.6) one may rewrite Eq. (C.1) as

$$\frac{p_4}{p_1} = G(1 + \beta M_3)^{\gamma_4/\beta} \left(\frac{7 M_s^2 - 1}{6}\right) \qquad (C.7)$$

where

$$G = \frac{A_1}{A_4}\frac{M_{3'}}{M_{4'}}\left[\frac{1 + \beta M_{3'}^2}{1 + \beta M_{4'}^2}\right]^{\frac{1}{2}} \left[\frac{1 + \beta M_{4'}}{1 + \beta M_{3'}}\right]^{\gamma_4/\beta} \qquad (C.8)$$

The factor G is the inverse of the so-called "effective gain factor", g which was first defined in Ref. 7 and is a constant depending only on the driver gas and on geometry.

The flow Mach number M_3 may be expressed as

$$M_3 = \frac{u_3}{a_3} = \frac{u_2}{a_3} = \frac{u_2}{a_1} \cdot \frac{a_1}{a_4} \cdot \frac{a_4}{a_{4'}} \cdot \frac{a_{4'}}{a_{3'}} \cdot \frac{a_{3'}}{a_3} \qquad (C.9)$$

which, after appropriate substitution, becomes

$$M_3 = \frac{1}{\frac{a_4/a_1}{u_2/a_1} G^{-\beta/\gamma_4} - \beta} \qquad (C.10)$$

Eq. (C.7) may now be rewritten as

$$\frac{p_4}{p_1} = G\left[1 + \frac{\beta}{\frac{a_4/a_1}{u_2/a_1} G^{-\beta/\gamma_4} - \beta}\right]^{\gamma_4/\beta} \frac{7 M_s^2 - 1}{6} \qquad (C.11)$$

For a conventional, constant-area shock tube, G = 1, and Eq. (C. 11) reduces to its standard form given by

$$\frac{p_4}{p_1} = \left[1 - \beta\left(\frac{u_2}{a_1}\right)\left(\frac{a_1}{a_4}\right)\right]^{-2\gamma_4/\beta} \frac{7\,M_s^2 - 1}{6} \qquad \text{(C. 12)}$$

Up to this point we have considered only the case of a single flow obstacle located at the diaphragm station. If one considers the possibility of having several flow obstacles as shown in Fig. C. 3 (see also Fig. 7) then it becomes necessary to make some additional assumptions about the nature of the flow. Two simple approaches for this situation have been considered.

In the first approach, which is perhaps somewhat naive, one may assume that the flow always becomes choked (in an isentropic manner) at the first minimum area and is supersonic thereafter, undergoing isentropic compressions and expansions through the succeeding flow obstacles. Since in the present work all of the minimum cross-section areas are equal, and similarly for the maximum areas ($A_4 = A_1 = A_{max}$), this would mean that the flow would become sonic in the first obstacle and undergo a supersonic expansion downstream of it. The flow would then decelerate (isentropically) back to a sonic condition in the second flow obstacle and again expand supersonically downstream of it, and so on for the next obstacle. Hence, for this situation, one only needs to consider the effect of the first obstacle since the succeeding ones are assumed to provide equal isentropic compressions and expansions, thus always producing the same flow Mach number downstream of all obstacles.

In the second approach, the other extreme was taken. It was assumed that the flow always becomes choked in the last obstacle and is subsonic through all preceding obstacles. The flow through each obstacle prior to the last one is assumed to accelerate (isentropically) to a subsonic speed corresponding to the passage area of the obstacle and then to decelerate at a constant pressure to a speed corresponding to the maximum cross-section area downstream of the obstacle, and so on.

When only a single flow obstacle is considered the two approaches, of course, become synonomous. Also, the value of M_3' does not depend on the approach taken since it is fixed by A^*/A_1, which is the same for all obstacles in the present work. In the second approach, one starts with this value of M_3' and proceeds backwards (i.e., upstream) through the obstacles to calculate a value for M_4'. Hence, the factor G given by Eq. (C. 8) will, in this approach, also depend on the number of flow obstacles considered. For a single flow obstacle, one gets a value for G equal to 1. 153, whereas for the case of three flow obstacles,

G = 1.408. The calculated performance curves based on these values are given in Figs. 8 and 9. (The relevant Mach numbers through the obstacles are given in Table C.1, for reference.)

The limiting condition that must be satisfied for the above results to be valid is that $M_{3'} < M_3$ in order for a left-running rarefaction wave to exist between the last flow obstacle and the contact surface. This requirement thus fixes a lower limit on the shock Mach number below which Eq. (C.11) may not be used. For the present case, this limiting value is found to be $(M_s)_{M_3 = M_{3'}} = 5.07$. For M_s less than the foregoing, conditions have to be matched using an upstream-facing shock wave or compression wave. This case is treated in Ref. 5, but is not of interest in the present work.

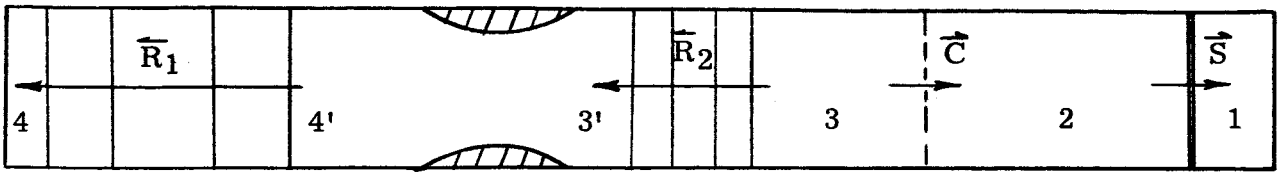

FIG. C. 1 SCHEMATIC OF SHOCK TUBE FLOW PATTERN

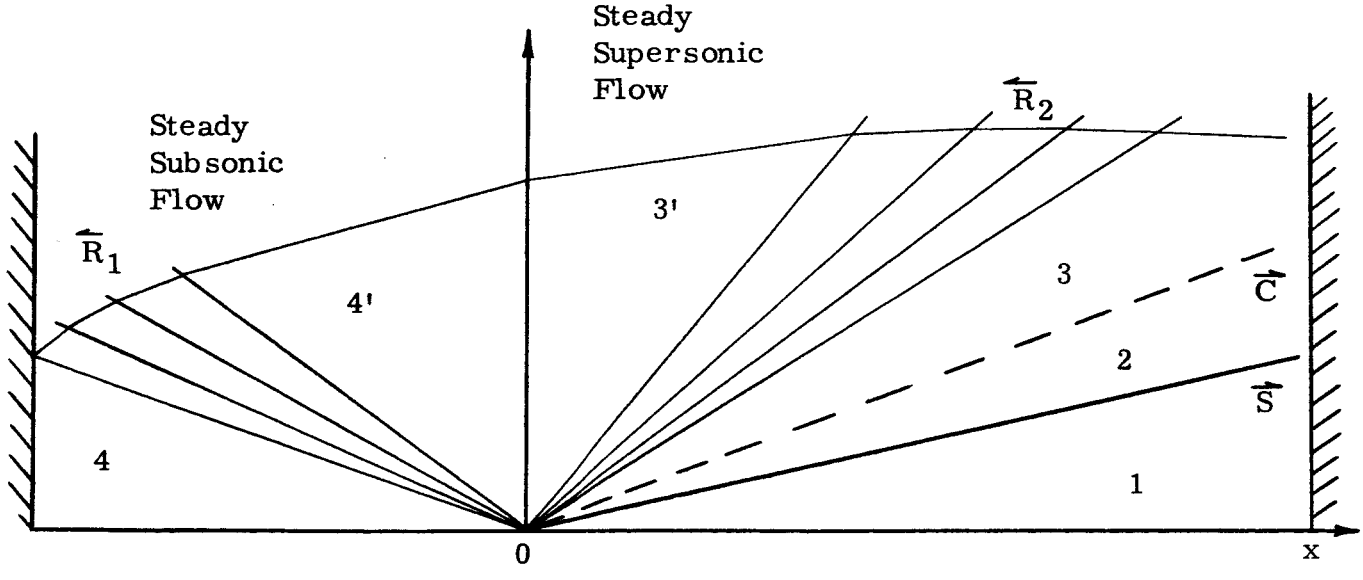

FIG. C. 2 WAVE DIAGRAM FOR SHOCK TUBE FLOW

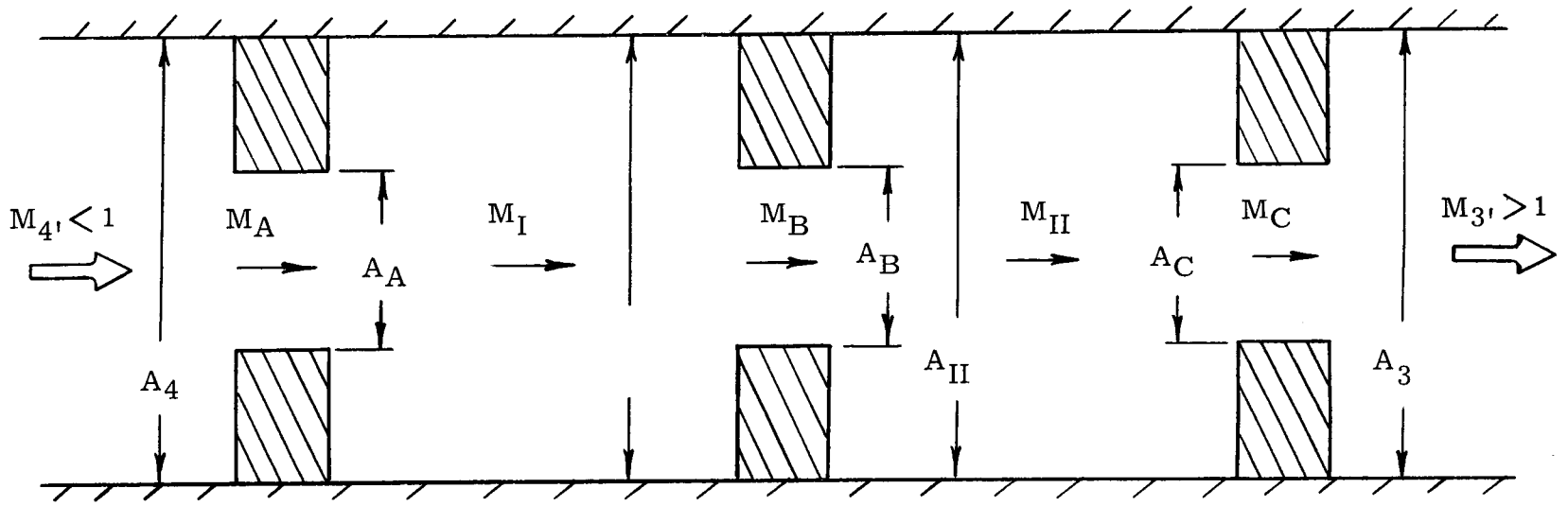

FIG. C. 3 SCHEMATIC OF THEORETICAL SYSTEM OF FLOW OBSTACLES

TABLE C.1

CALCULATED VALUES OF FLOW MACH NUMBERS

AND FACTOR G FOR VARIOUS TRAP ARRANGEMENTS

Number of Traps	$M_{4'}$	M_A	M_I	M_B	M_{II}	M_C	$M_{3'}$	G
1	.322	1	-	-	-	-	2.19	1.153
2	.265	.593	.322	1	-	-	2.19	1.298
3	.232	.495	.265	.593	.322	1	2.19	1.408